Technical Paper
J. Astron. Space Sci. 37(2), 143-156 (2020)
https://doi.org/10.5140/JASS.2020.37.2.143

JASS Journal of Astronomy and Space Sciences

Observations of the Polar Ionosphere by the Vertical Incidence Pulsed Ionospheric Radar at Jang Bogo Station, Antarctica

Young-Bae Ham[1,2], Geonhwa Jee[1,2†], Changsup Lee[1], Hyuk-Jin Kwon[3], Jeong-Han Kim[1], Nikolay Zabotin[4], Terence Bullett[4]

[1]Korea Polar Research Institute, Incheon 21990, Korea
[2]University of Science and Technology, Daejeon 34113, Korea
[3]School of Space Research, Kyung Hee University, Yongin 17104, Korea
[4]Cooperative Institute for Research in Environmental Sciences, University of Colorado Boulder, Boulder, Colorado 80309, USA

Korea Polar Research Institute (KOPRI) installed an ionospheric sounding radar system called Vertical Incidence Pulsed Ionospheric Radar (VIPIR) at Jang Bogo Station (JBS) in 2015 in order to routinely monitor the state of the ionosphere in the auroral oval and polar cap regions. Since 2017, after two-year test operation, it has been continuously operated to produce various ionospheric parameters. In this article, we will introduce the characteristics of the JBS-VIPIR observations and possible applications of the data for the study on the polar ionosphere. The JBS-VIPIR utilizes a log periodic transmit antenna that transmits 0.5–25 MHz radio waves, and a receiving array of 8 dipole antennas. It is operated in the Dynasonde B-mode pulse scheme and utilizes the 3-D inversion program, called NeXtYZ, for the data acquisition and processing, instead of the conventional 1-D inversion procedure as used in the most of digisonde observations. The JBS-VIPIR outputs include the height profiles of the electron density, ionospheric tilts, and ion drifts with a 2-minute temporal resolution in the bottomside ionosphere. With these observations, possible research applications will be briefly described in combination with other observations for the aurora, the neutral atmosphere and the magnetosphere simultaneously conducted at JBS.

Keywords: Vertical Incidence Pulsed Ionospheric Radar (VIPIR), polar ionosphere, Jang Bogo Station, Antarctica

1. INTRODUCTION

The polar ionosphere is the region of the upper atmosphere approximately from 90 to 1,000 km altitude and strongly influenced by the solar wind through the magnetosphere in the polar region. This region of the ionosphere is characterized by the polar cap region, where the geomagnetic field lines are open and directly connected to the solar wind, and the auroral region, where the field lines are closed and map to the plasma sheet in the magnetosphere (Sergeev 1990). The polar ionosphere plays a crucial role in the energy transfer from the Sun to the Earth's atmosphere via the solar wind-magnetosphere-ionosphere interactions. When the solar wind meets the magnetosphere the solar wind energy is partially transmitted into the magnetosphere and the accumulated energy in the magnetosphere is initially dissipated in the polar ionosphere with various forms and then transferred to the thermosphere via ion-neutral coupling processes. The solar wind-magnetospheric energy deposited in the polar upper atmosphere is subsequently transmitted to the lower latitudes in the form of the neutral winds or neutral/ionospheric disturbances. On the other hand, the polar ionosphere does not passively respond to the magnetospheric energy inputs but actively acts to affect the magnetosphere in a significant way (Heelis 1982; Russell 2000; Lu et al. 2016). Therefore, it is indispensable to constantly monitor the state of the polar ionosphere to understand not only the polar ionosphere itself but also the energy

Received 22 MAY 2020 **Revised** 1 JUN 2020 **Accepted** 3 JUN 2020
†**Corresponding Author**
Tel: +82-32-760-5306, E-mail: ghjee@kopri.re.kr
ORCID: https://orcid.org/0000-0001-7996-0482

exchanges between the polar ionosphere and the magnetosphere. Currently a number of ground-based observations for the polar ionosphere have been operating in the polar region. First of all, there exist several incoherent scatter radars (ISRs) in the polar region such as EISCAT and AMISR in the Arctic and PANSY in Antarctica in order to observe the polar ionosphere in the most versatile way (Rishbeth & Eyken 1993; Valentic et al. 2013; Sato et al. 2014). The ISR is one of the most powerful instruments for monitoring the ionosphere which is capable of observing the height profiles of various ionospheric parameters such as plasma density, ion drift, and electron and ion temperatures over the entire ionospheric region regardless of the level of geomagnetic disturbance. However, its operation is very expensive and requires large hardware facilities, which is not suitable for the locations like in Antarctica. Another instrument widely used for the observations of the ionosphere is the Super Dual Auroral Radar Network (SuperDARN) that is extensively operating mainly in the polar region but also in the mid-latitude region to provide two dimensional structures of the ionospheric irregularity as well as plasma convection in the polar region (Chisham et al. 2007; Lester 2014). But this radar is limited to observe only the ionospheric irregularities rather than regular ionospheric density parameters. Finally, the ionospheric sounding system such as digisonde has conventionally been operating to monitor the bottom side ionosphere in the global scale (Reinisch & Galkin 2011). All these ionospheric observations are most intensively performed in the Arctic, but there have been relatively limited observations in Antarctica mainly due to the very restricted accessibility to the region.

JBS, the second Korean Antarctic station established in 2014, is located near the boundary region between the auroral zone and the polar cap depending on local time and geomagnetic activity level, and its location is ideal for monitoring the polar ionosphere. Korea Polar Research Institute (KOPRI) has been operating several optical and radar instruments at JBS to simultaneously monitor the various aspects of the polar upper atmosphere. In 2014, the Fabry-Perot Interferometer (FPI) was first installed in collaboration with NCAR/HAO to measure the thermospheric winds and temperature in the polar cap and auroral region (Lee et al. 2017; Wu et al. 2017). In the following year, the installation of the Vertical Pulsed Ionospheric Radar at Jang Bogo Station (JBS-VIPIR) was initiated and completed in 2017 in collaboration with University of Colorado (Boulder) to start observing the polar ionosphere over JBS. In addition to using FPI and VIPIR, a number of ground-based observations have been simultaneously performed to monitor the various aspects of the space environment in the polar region. These include search-coil magnetometer (SCM) and dIdD suspended system vector magnetometer for the magnetospheric observations, GPS TEC/Scintillation monitor for the ionospheric irregularity, All Sky Cameras for the airglow emissions as well as the aurora, and neutron monitor for energetic particles and cosmic ray (Kim et al. 2018; Kwon et al. 2018). In this article, the JBS-VIPIR observations for the polar ionosphere will be introduced with possible applications for the research in the polar region.

2. DIGISONDE VS. DYNASONDE

The JBS-VIPIR is operated with the Dynasonde which is distinguished from more conventional digital ionosonde. Before introducing the JBS-VIPIR observations, it is worthwhile to describe the differences between the Dynasonde and the digital ionosondes. Ionosondes are radars using radio pulses to detect the ions in the ionosphere, which was conceived for the purpose of measuring the height of the ionosphere in 1925 by Breit & Tuve (1925). Pulsed radio waves of up to about 20 MHz are reflected from the ions, providing various information of the state of the ionosphere. The ionosphere is dispersive or frequency-dependent medium, each frequency being reflected by specific ionization densities. Physical properties of an echo such as travel time, phase, polarization, direction of arrival, amplitude, and Doppler are significantly modified by ionospheric properties below and near the reflection level. Therefore, it is possible to obtain various information of the ionospheric properties by careful measurements and analysis of the properties of the reflected radio echoes. The ionograms produced by the ionosondes are the graphical images of pulse travel time vs. radio frequency. It is relatively simple to estimate layer peak ionization densities from them but the estimation of the actual height of the ionospheric layers is a lot more difficult and requires extensive inversion procedures. However, there is a great deal of additional information on the ionosphere which cannot be included in the graphical images of the ionograms.

Currently, there is only one alternative ionospheric sounding system supplied with a fully autonomous data processing capability: Dynasonde. The Dynasonde is originally developed as an ionosonde capable of measuring "the dynamics of the ionosphere" and it provides the hardware and software resources to accomplish complete characterizations of the radio echoes available by sounding throughout the whole frequency bands of 0–30 MHz. Radio pulses in the Dynasonde are transmitted in groups in carefully designed pulse set patterns with small frequency

offsets. The reflected echoes are recognized in real time by algorithms that effectively discard false echoes and identify the time-of-arrival values with complex amplitudes. This information is transformed into physical parameters such as echo locations, a line-of-sight (LOS) Doppler velocity, one or more echo polarization parameters, average phase value, echo peak amplitude, and several other echo characteristics. It is important to note that there is a fundamental difference between the Dynasonde and other ionosonde concepts. The data acquisition procedures in the Dynasonde are performed with minimized assumptions and no application of data pre-processing (e.g., Fast Fourier transform) as in one of the popular ionosonde designs that suffer from the loss of precision of physical parameters such as spatial resolution and angles of arrival. An echo is an echo; it is not a selected Doppler peak following FFT processing. It is not even simply an amplitude peak. When amplitude is used to recognize echoes, it is the required time-of-arrival consistency among amplitude peaks within the pulse set which rejects false echoes and identifies true echoes. These established data acquisition strategies utilize most of the hardware resources of the Dynasonde, in addition to fully programmable control of each of these features (NOAA National Centers for Environmental Information 2016).

3. VERTICAL INCIDENCE PULSED IONOSPHERIC RADAR (VIPIR)

VIPIR is an ionospheric radio sounding system operated with the Dynasonde for data acquisition and processing to obtain the height profiles of electron density, ion drift, and ionospheric tilts. It was installed at JBS in February 2015 in collaboration with the Cooperative Institute for Research in Environmental Sciences (CIRES), University of Colorado Boulder, USA. Due to the harsh Antarctic environment with strong wind and cold temperature at JBS, however, it did not properly operate to produce observational data until 2017 after the two-year test operation with the improvements of transmit antenna towers. The JBS-VIPIR uses HF radar system with a digital RF technology developed by Scion Associates Inc. and the comprehensive data processing software suite Dynasonde developed by Dynasonde Solutions. Please see Table 1 for the specification of the radar. The transmit antenna in the JBS-VIPIR uses an inverted log periodic antenna (LPA) transmitting 0.5 to 25 MHz HF radio waves. It consists of about 1.5 km of radiating wires in four zig-zag planes with four 36-m towers on a square of 75 m per side (Fig. 1). The advantage of this type of transmit antenna is to provide very uniform beam pattern for all frequencies compared to the traditional delta antenna (Australian Government Bureau of Meteorology 1998; Bullett & Redmon 2008). The receiving antenna consists of an array of 8 orthogonal 4-m active dipole antenna. The configuration of the antenna is illustrated in Fig. 2. Also shown is the photo of the JBS-VIPIR antenna system and the radar electronics in Fig. 3 and Fig. 4, respectively. The JBS-VIPIR is the first ionospheric sounding system using the Dyansonde data analysis approach to observe the ionosphere in the polar cap and/or auroral region in Antarctica.

4. DATA PROCESSING PROCEDURE IN THE DYNASONDE

The principles of Dynasonde sounding and data processing procedures are based on the radio echoes which are defined by seven precisely determined parameters with each individual error estimate. These include two angles of arrival, group range, Doppler, polarization, phase range, and amplitude which are produced with their individual error estimates. The Dynasonde uses short sequences of narrowband pulses. In these pulse sets, the radio frequencies are slightly offset by 1–4 kHz from the base frequency in a carefully designed pattern to enable precision range measurements within a few tens of meters. The phase and amplitude of received echoes are directly used to derive physical properties of the raw data, instead of traditional

Table 1. Specifications of the JBS-VIPIR

VIPIR Mark I Radar	Upgrades for VIPIR Mark II
• Very high interference immunity: IP3 > 45 dBm • High dynamic range: 115(I) + 30(V) dB • Direct RF sampling 14 bits at 80 MHz • Fully digital conversion, receiver and exciter • USB-2 data and command/control interfaces • 8 coherent receive channels; Frequency: 0.3–25 MHz • 4 kW class AB pulse amplifier: 3rd harmonic < –30 dBc • Precise GPS timing for bi-static operation • Radar software Open Source C code; runs under Linux	• FPGA based digital receiver • 16 bit, 120 MHz ADC • USB-3 data transfer • 32 bit I/Q data • Improved analog front end • Improved receive antenna pre-amplifiers • Contemporary computers and data storage • Options: - High power low pass transmit harmonic filter - Rubidium oscillator for oblique phase measurements

JBS-VIPIR, Jang Bogo station-vertical incidence pulsed ionospheric radar.

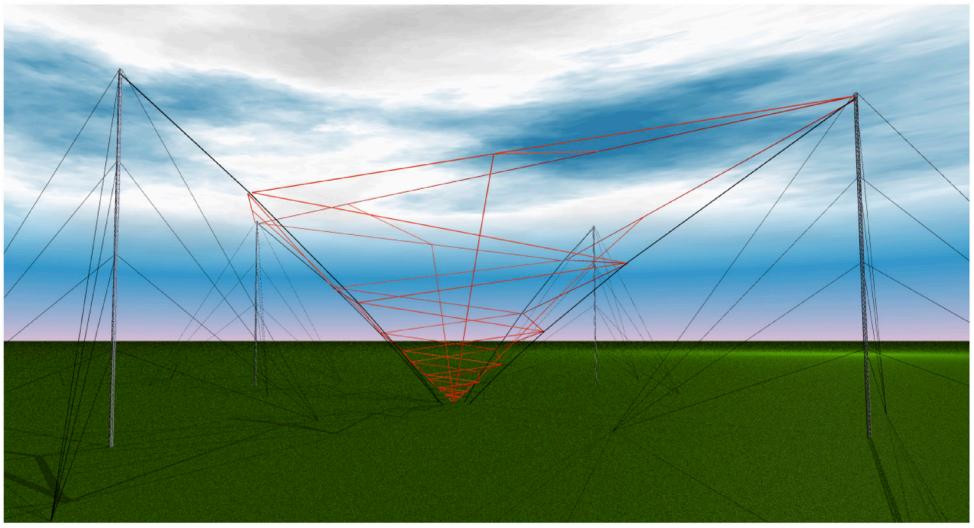

Fig. 1. Illustration of the VIPIR transmit antenna. The zig-zag radiating wires (red) are supported by four 36-m towers. Adopted from Bullett & Redmon (2008) with permission of author.

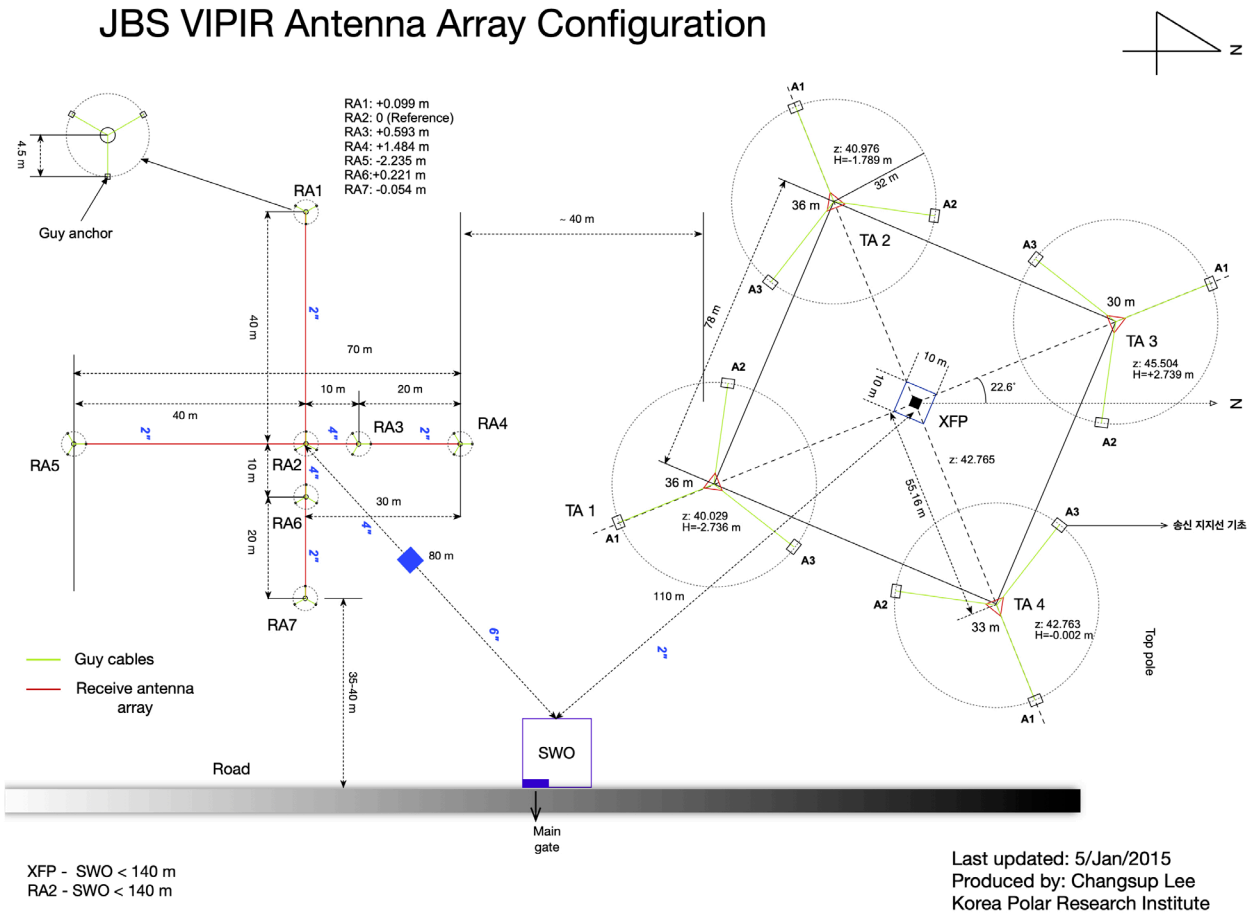

Fig. 2. Antenna configuration of the JBS-VIPIR ionospheric sounding system. JBS-VIPIR, Jang Bogo station-vertical incidence pulsed ionospheric radar.

amplitude-based image analysis used in Digisonde (Negrea et al. 2016). The Dynasonde can be operated in three different modes and each mode has a different scheme for transmitting pulses. The operation modes available for

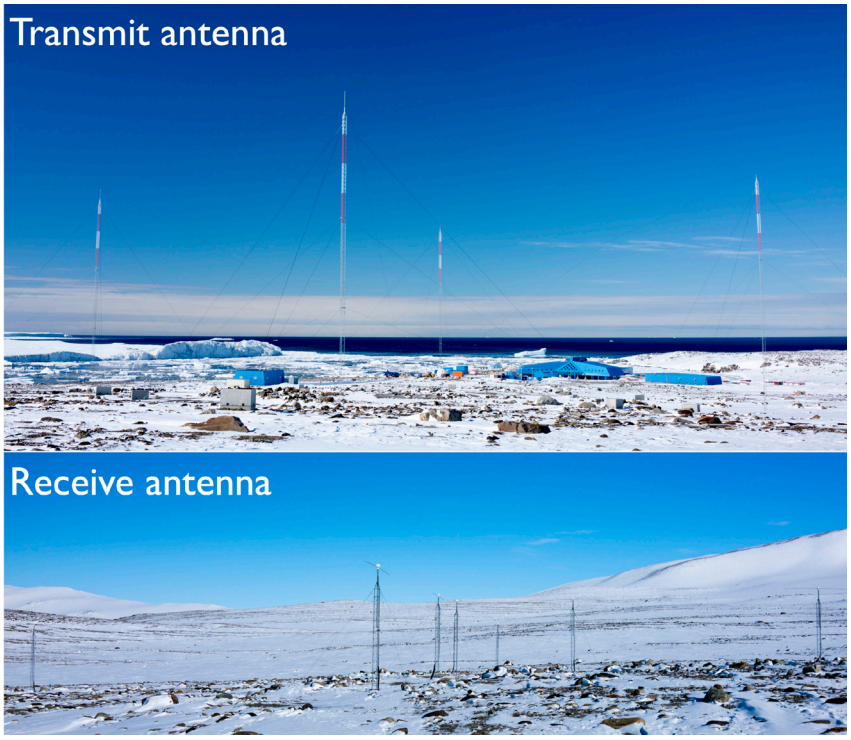

Fig. 3. Photos of the JBS-VIPIR antenna system. Four 36-m towers for the transmitting antenna and 76-m towers for the receiving antenna are displayed. JBS-VIPIR, Jang Bogo station-vertical incidence pulsed ionospheric radar.

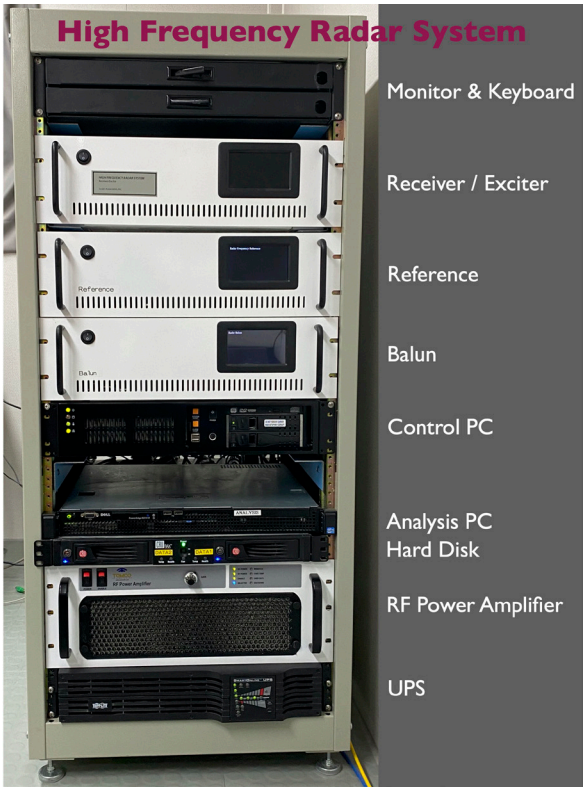

Fig. 4. High frequency radar electronics is composed of receiver/exciter, reference, balun, RF power amplifier and control and analysis PCs.

Dynasonde are ionogram mode (I-mode), kinesonde mode (K-mode), and basic measurement set mode (B-mode). In I-mode, the pulses are transmitted by monotonically increasing the base frequency, which can generate conventional ionogram with high frequency resolution. But the Doppler measurement cannot be achieved in I-mode. In K-mode, there are a few base frequencies that are chosen by the user and these base frequencies are repeated several times. K-mode offers high temporal resolution within a single frequency, thus being able to give Doppler measurement. B-mode is a compromise between I-mode and K-mode. The pulses are transmitted in six sequential frequencies and these six frequencies are repeated six times. This six by six set is called 'Block'. After one block finishes, the next blocks with higher frequencies are followed (Wright & Pitteway 1979a). In B-mode, both conventional ionogram and Doppler measurement can be achieved simultaneously. The Dynasonde of the JBS-VIPIR has been operated in B-mode with a 2-min temporal resolution. The recorded In-phase and Quadrature signals achieved by each sounding session are analyzed by the Dynasonde software. At the first stage, an echo recognition procedure is performed to reject false echoes and noise. Each recognized echo has physical parameters such as amplitude, polarization, two angles of arrival, stationary phase group range, average phase, and

error estimates.

Because the refraction index of the ionosphere increases as the electron density increases (and the electron density largely increases as the height increases in the bottom side ionosphere), the velocity of the radio waves becomes slower as they propagate to higher altitude with higher density in the ionosphere. The slowing radio waves eventually stop to move forward and are reflected back to the ground when they meet the critical level of the ionospheric density for a given radio wave frequency. The travel range of the waves can be readily calculated from the time interval between transmission and reception of the radar with the speed of light c, which is called a virtual range and normally greater than true travel distance of the wave. To derive the true heights of the ionospheric layers with corresponding densities requires an inversion procedure of the ionosonde data. The inversion procedure in the conventional ionosonde such as Digisonde mostly adopts the assumption of a horizontally plane-stratified ionosphere to ignore horizontal gradients for the simplifications of the problem. However, the real ionospheric density structure is significantly different from the simplified vertical ionosphere but various sources cause horizontal gradients of the ionospheric density throughout a wide range of spatial and temporal scales and magnitudes. These include solar terminator effects near sunrise and sunset, gravity waves, traveling ionospheric disturbances, storm-time density variations, energetic particle precipitation, plasma bubbles, equatorial anomaly etc. Therefore, the measurements with the conventional inversion procedure should consequently be in disagreement with the real ionosphere. In order to overcome this limitation, a new inversion scheme called NeXtYZ (pronounced 'next wise') is adopted for the JBS-Dynasonde. In the NeXtYZ inversion scheme, the Wedge-Stratified ionosphere (WSI) model is applied instead of the plane-stratified ionosphere model as described earlier. With the WSI model, the NeXtYZ performs ionogram inversion by a numerical ray-tracing and least squares optimization procedure to derive horizontal gradients as well as vertical electron density profile. This means that three-dimensional electron density profiles can be obtained from the NeXtYZ inversion procedure. The horizontal gradients of the ionospheric electron density are represented by so-called "the ionospheric tilts" and determined by the two horizontal components of the unit normal vector of the constant electron density surface in the WSI model (Negrea et al. 2016).

The NeXtYZ is a three-dimensional ionogram inversion program that retrieves electron density profile resulting in the recorded ionogram. WSI model assumes that the plasma density is constant on each plane, and the planes do not intersect inside the ionosonde's field of view. It sequentially determines the height and the orientation (west-east and south-north tilts) of each constant plasma density surface, and it is performed from bottom to top. The first layer is determined by an ionization model developed by Titheridge. It is physics-based model and gives missing information of the ionospheric layer below the minimum height that can be detected by the ionosonde (It is also used for the undetectable E-F valley region). This information affects the accuracy of the inversion results. Once the first layer is set the process of sequential determination of the next layers begins and it consists of numerical ray tracing and least squares optimization procedure. The ray tracing simulates the trajectories of the rays that resulted in echoes in the current wedge (the region between the previous and the next layers), and it is sensitive to the parameters of the next layer. The optimization procedure determines the parameters by minimizing the residual between calculated and observed echo group ranges and the distance between the location of the initial launch of the rays and the ground return point. The angles of arrival of echoes are used as initial conditions for the ray tracing, and at least 10 ionosonde echoes are needed for the current wedge. The ray tracing and optimization procedure is performed in iterative manner (Zabotin et al. 2006).

With the WSI model and the NeXtYZ inversion program the Dynasonde can derive 3-D electron density profiles within the ionosonde field of view, but the 3-D electron density profiles are also available through digisonde system. The raw digisonde ionograms are automatically scaled and the electron density profile for each ionogram is achieved by finding polynomial curves corresponding to the electron density profile that can reproduce the measured h'(f) trace. Because ordinary vertical echoes are used only for the automatic scaling, the derived profile is vertical profile. Huang & Reinisch (2006) described a method of deriving 3-D electron density distribution from the single station digisonde data. To determine 3-D distribution of the electron density from digisonde data, vertical electron density profiles and local tilts are required and the local tilts are calculated from the digisonde skymap. The skymap is a representation of echolocations in a zenith-azimuth angle grid. A local tilt corresponds to the zenith and azimuth angles of the center of the echo distribution in the middle of the F2 layer. A 3-D density distribution is constructed to reproduce the measured vertical electron density profile and tilt at the sounder location, and Comité Consultatif International des Radiocommunications (CCIR) or Union Radio Scientifique Internationale (URSI) coefficients are used for the mapping of ionospheric characteristics. However, note that the tilts for 3-D density distribution are obtained only for F2 layer, which may not

be maintained in the lower ionosphere. In contrast, the 3-D density distribution derived by the NeXtYZ allows the tilts to vary with height since the tilts are determined by numerical ray tracing for each wedged plane.

5. DYNASONDE IONOGRAM

Fig. 5 shows the ionogram image achieved by the JBS-VIPIR. The upper panel is a typical representation of the

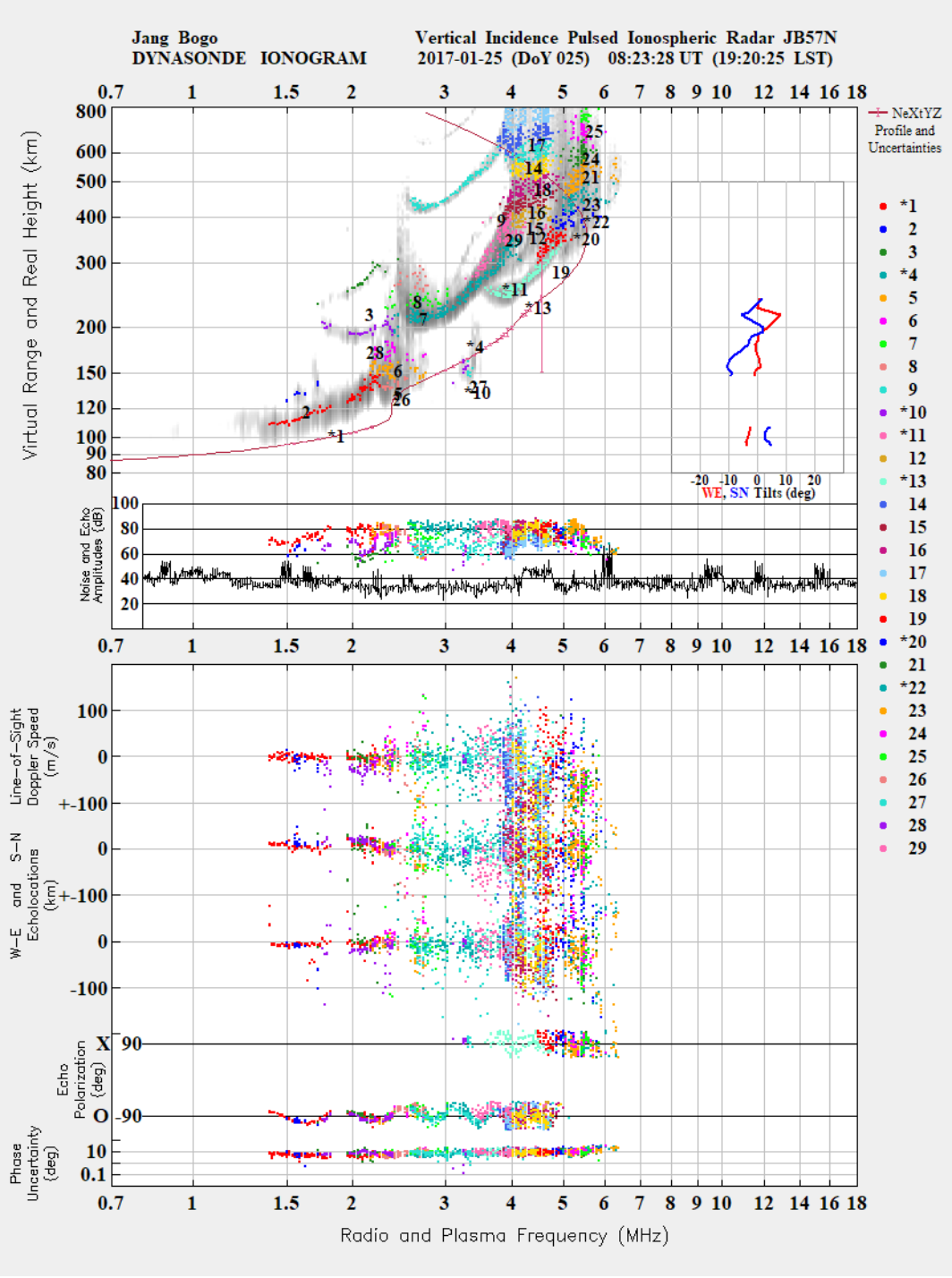

Fig. 5. Ionogram image (top) in the standard Dynasonde presentation format. Also shown at the bottom panel are Doppler, echolocations, polarization, and error parameter. Echo group range versus radio frequency appears in the logarithmic scales. Colored dots in the figure denote echo traces. The inset of the top panel shows the meridional (blue) and zonal (red) local tilt angles of each constant plasma density plane.

ionosonde results. The gray-scaled contour is the amplitude of the raw Signal-to-Nosie Ratio. Echoes identified by the echo recognition procedure is represented by 29 different colored dots with numbers. Groups of echoes with similar physical parameters are designated to be a trace with same colors. The echo amplitudes and the background noise level are plotted at the bottom of the panel. The magenta curve is the electron density profile derived from the NeXtYZ with the height error estimates presented by the vertical error bars along the profile. The NeXtYZ-derived height profiles of the ionospheric tilts are also presented at the insert panel on the right. They represent the tilt angles of the local wedge reflection plane in the east-west (red) and north-south (blue) directions. Note that only 7 out of 29 traces marked with asterisk are used to solve the inversion problem in the NeXtYZ. The lower panel of Fig. 5 shows the additional parameters of the individual echoes determined by the Dynasonde software including LOS Doppler speed, zonal and meridional components of echo locations, phase uncertainty and echo polarization, which are all related to the phase measurements.

6. PHASE MEASUREMENTS

Phase information can be achieved by constructing receiver as an array of multiple antennas. Wright & Pitteway (1979b) described the data processing of the Dynasonde phase measurements achieved by receiving array of four dipole antennas, where the four antennas are orthogonally aligned with east-west and north-south directions as shown in Fig. 6. In this figure, ϕ_0 is the phase at the center of the array. As mentioned earlier, a few kHz frequency shift (Δf) from the base frequency (f) is applied to form a pulse set. ϕ' and ϕ'' are the measured quantities at f and f + Δf, respectively and related to various phase shifts by the equations shown on the figure. ϕ_F is the phase shift resulting from the frequency shift Δf (i.e., $\phi_F = \phi'' - \phi'$) and appears approximately equally at all antennas. ϕ_X and ϕ_Y are the phase shifts caused by reflected waves coming from the off-zenith zonal and meridional directions, respectively, which will be used to determine the echolocations. In the presence of the magnetic field, the ionosphere acts as a birefringent medium. The polarization of the electromagnetic wave is changed as they propagate through the ionosphere, which is represented by ϕ_P. The phase shift ϕ_P appears in the east-west direction and also related to the orthogonality to the north-south direction. For a single dipole antenna it is straightforward to determine ϕ_F by $\phi'' - \phi'$ but the mean value of the differences from the four antennas is taken for ϕ_F estimation. Because ϕ_F is just a result of frequency shift to form a pulse set, ϕ_F-free phases (ϕ_W, ϕ_E, ϕ_S, and ϕ_N) are calculated by averaging each ϕ' and $\phi'' - \phi_F$ pair. ϕ_X and ϕ_Y can be given by

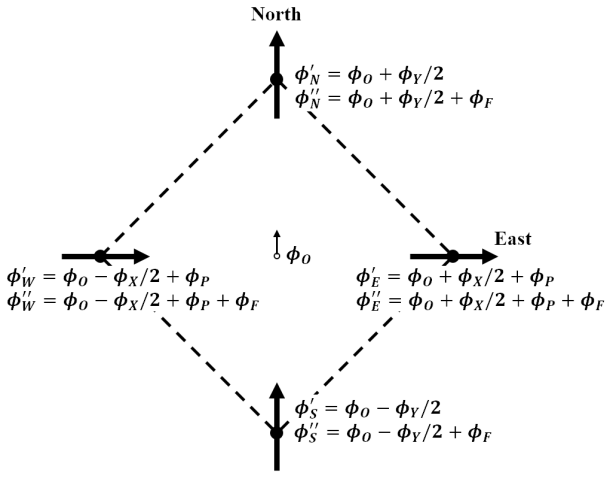

Fig. 6. Schematic representation of the Dynasonde receiving array and echo phase information adopted from Wright & Pitteway (1979b). Arrows at corners of the square array represent dipole lengths and directions. Primed phases are measured at f and double primed phases at f + Δf. Adopted from Wright & Pitteway (1979b) with AGU permission policy.

$$\phi_X = \phi_E - \phi_W \tag{1}$$

$$\phi_Y = \phi_N - \phi_S \tag{2}$$

Now the orthogonal components of the echolocations can be calculated by

$$x = h' \lambda \phi_X / 2\pi D_x \tag{3}$$

$$y = h' \lambda \phi_Y / 2\pi D_y \tag{4}$$

where x and y are the east-west and north-south echolocations, h′ is a virtual range, λ is a transmitted radio wave frequency, and D_x and D_y are the antenna separation distances in the east-west and north-south pairs, respectively. The echo polarization (ϕ_P) is the differences between the mean values of the north-south and the east-west phases:

$$\phi_P = (\phi_N + \phi_S) / 2 - (\phi_E + \phi_W) / 2 \tag{5}$$

and is approximately 90° for X-mode echo and –90° for O-mode echo.

The motion of the reflection surface generates temporal changes of the phase. Because the Dynasonde B-mode repeats pulse sets with the same frequency, the change of the phase ($\Delta\phi$) can be measured for a short time interval

(Δt). In other words, $\Delta\phi$ is the phase difference between the pulse sets repeated at the same base frequency and caused by the motion of the reflection layer during time interval Δt. The LOS Doppler speed (V^*) can then be calculated from this temporal changes of the phase as

$$V^* = \frac{c}{4\pi f}\frac{\Delta\phi}{\Delta t} \quad (6)$$

where c is the speed of light and f is the wave frequency.

7. MAIN IONOSPHERIC PARAMETERS FROM THE JBS-VIPIR OBSERVATIONS

7.1 Electron Density Profiles

The local time variations of the monthly averaged electron density profiles are presented in Fig. 7 during June (winter), September (spring), and December (summer). The electron density is largest in summer but smallest in winter as expected from the solar zenith angle variations. The overall diurnal variations are relatively small both in winter and summer since the upper atmosphere is nearly in the dark (June) or sunlit (December) condition. On the other hand, during spring equinox when there are both daytime and nighttime, a clear diurnal variation exists with the maximum electron density near the local noon and minimum at the local midnight. The top boundary of the density profiles, which corresponds to the F-region peak, in spring equinox also shows a typical diurnal variation of daytime minimum and nighttime maximum. Note that there is a noticeable density structure near the bottom of the profile during nighttime in winter and spring. The nighttime density enhancements at the bottom of the profiles should be related to the auroral particle precipitation occurring near the auroral region. The data vacancy above the enhancement indicates that there is a valley between the E-region density enhancement and the F-region density. There is also an indication of the valley during the daytime in spring and summer but it is related to the E-region density by solar production. The high-resolution measurement of the ionospheric electron density profile will provide valuable data not only for the study of the ionospheric density variations but also for various relevant researches such as the magnetosphere-ionosphere coupling, the ion-neutral coupling, and the auroral effects on the upper atmosphere in the polar region.

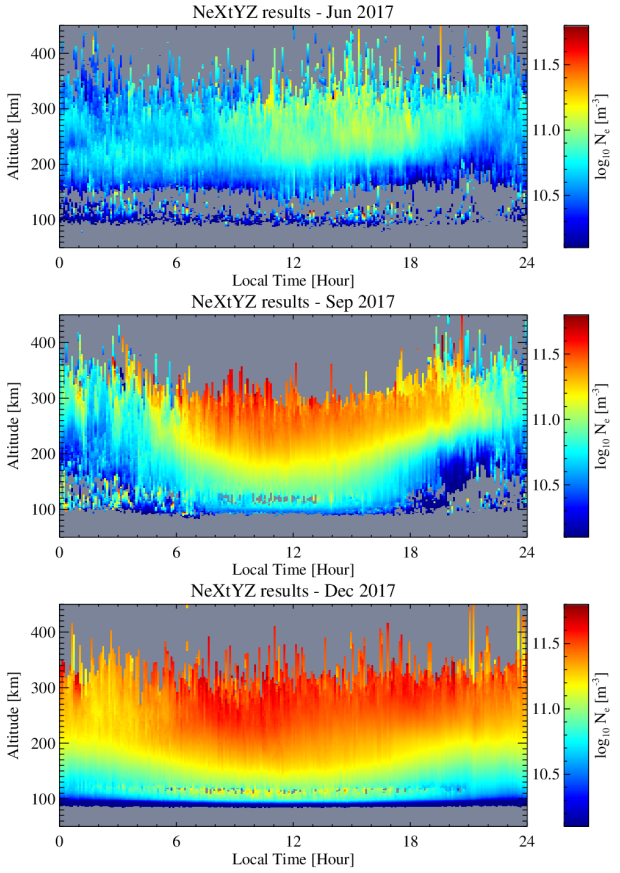

Fig. 7. Diurnal variations of the monthly mean electron density profiles obtained from the JBS-VIPIR for June (top), September (middle), and December (bottom) in 2017. JBS-VIPIR, Jang Bogo station-vertical incidence pulsed ionospheric radar.

7.2 Ionospheric Tilts

The wedge stratified ionosphere (WSI) model for NeXtYZ describes not only the vertical density variations but also the horizontal gradients of the density variations. The plasma density surfaces in the WSI model are represented locally for small increments in plasma frequency at a sequence of heights along the vertical axis by tilted sections of constant density planes. The slope of each plane is characterized by the unit normal vector, which defines the tilt of the ionospheric density. Fig. 8 shows the NeXtYZ tilts in the zonal (left) and meridional (right) directions. The NeXtYZ tilts indicate the angles between the vertical direction and the normal vector of the tilted ionospheric plane with a constant density. The local time variations of the monthly mean ionospheric tilts are presented in Fig. 8 for June (winter), September (spring), and December (summer) in 2017. It is hard to see any systematic variations in the zonal tilts in the left panels especially in summer. On the other hand, the meridional tilts in the right panels show clear diurnal variations in the F-region in equinox, which seems to be associated with the diurnal variations of the ionospheric density. Since the ionospheric tilts are known to be closely associated with

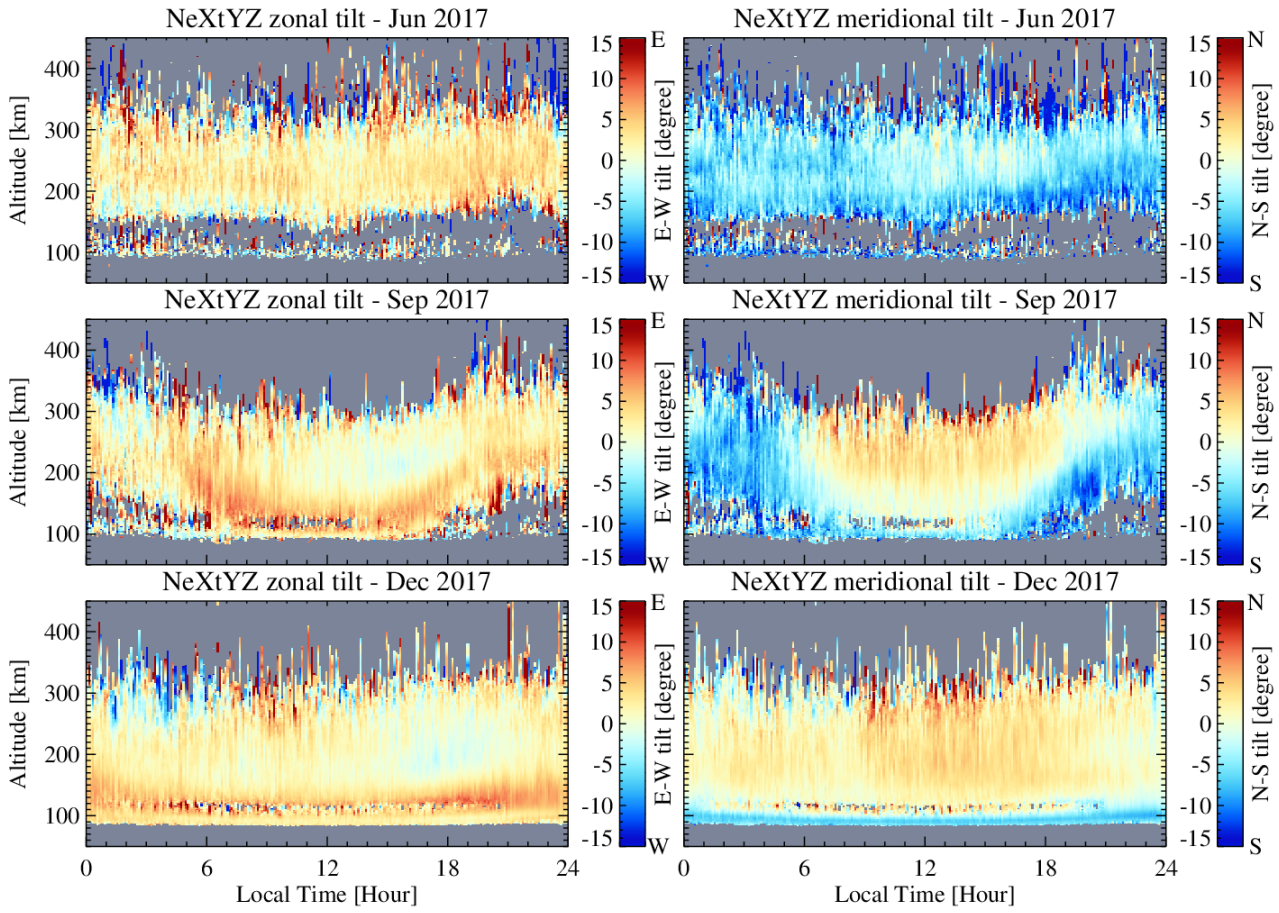

Fig. 8. Diurnal variations of the monthly mean ionospheric tilt profiles in the west-east (left) and south-north (right) directions for June (top), September (middle), and December (bottom) in 2017.

the ionospheric irregularities, the tilt data will be analyzed with the simultaneously monitored GPS scintillation data to study on the irregularities in the polar ionosphere, especially during the periods of auroral substorm.

7.3 Plasma Drift

The Doppler measurements of LOS speed can be used to derive the intrinsic plasma velocity of the ionosphere. Theoretically, if there are at least three different echoes which come from different locations, the plasma drift velocity can be derived from the LOS Doppler speed and three-dimensional echo locations by least square method. Fig. 9 illustrates the geometry of the LOS Doppler speed V^*, the drift velocity $\vec{v}$ and the unit vector $\hat{n}$ pointing the LOS direction, which are given by

$$V^* = \vec{v} \cdot \hat{n} \tag{7}$$

$$\vec{v} = v_x \hat{x} + v_y \hat{y} + v_z \hat{z} \tag{8}$$

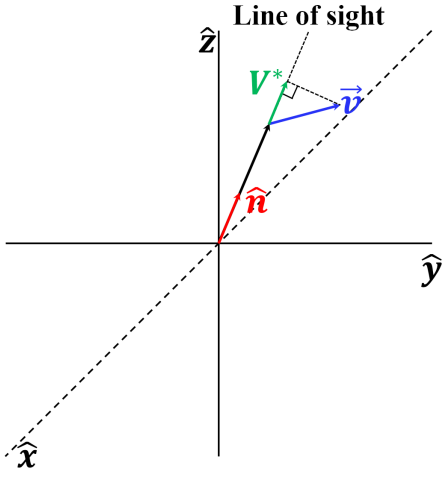

Fig. 9. Illustration of the line-of-sight (LOS) Doppler speed and the intrinsic velocity.

$$\hat{n} = n\ \hat{x} + n_y \hat{y} + n_z \hat{z} \tag{9}$$

Equation (7) is the model function for the least square

method. When the least square method is applied, the residual that needs to be minimized is

$$S = \sum_{i=1}^{N} \left[\left(v_x n_{xi} + v_y n_{yi} + v_z n_{zi} \right) - v_i^* \right]^2 \quad (10)$$

where V_i^* is the LOS Doppler speed for ith echo.

Fig. 10 shows monthly averaged meridional (right) and zonal (left) components of the ion drift velocity. The zonal and meridional directions indicate geographic east-west and north-south directions. For the estimation of the ion drift velocity, echoes were collected for each 20 km height bin in the height range from 80 to 280 km. The observed ion drifts show distinctive diurnal variations for both components, which reflect the two cell ionospheric convection pattern in the polar region. The typical directions are antisunward within the polar cap and sunward in the auroral region. These patterns appear as maximum ion drifts at terminators for zonal component and at noon and midnight for meridional component as shown in Fig. 10. There are marginal seasonal variations. Comparison of the Dynasonde ion drifts with the European Incoherent Scatter Radar (EISCAT) measurements of ion drift was conducted by Sedgemore et al. (1998) and it is confirmed that the Dynasonde ion drift is in a good agreement with the EISCAT measurements.

A number of studies reported the statistical patterns of the high-latitude ionospheric convection patterns for different interplanetary magnetic field (IMF) conditions. Fig. 11 shows the ion velocity vectors at 250 km altitude from the drift measurements for the negative (left) and positive (right) y-components of IMF for winter solstice, equinox, and summer solstice from top to bottom. Data with the transverse component of IMF (B_T) less than 5 nT were excluded for this figure. The hourly mean velocity vectors are presented at the magnetic latitude of JBS (~80° geomagnetic latitude). There are significant differences between the two different IMF conditions, which are associated with asymmetric magnetospheric currents and resulting plasma convection with IMF B_y component.

The ionospheric plasma convection is the characteristic phenomenon of the high-latitude ionosphere resulting from

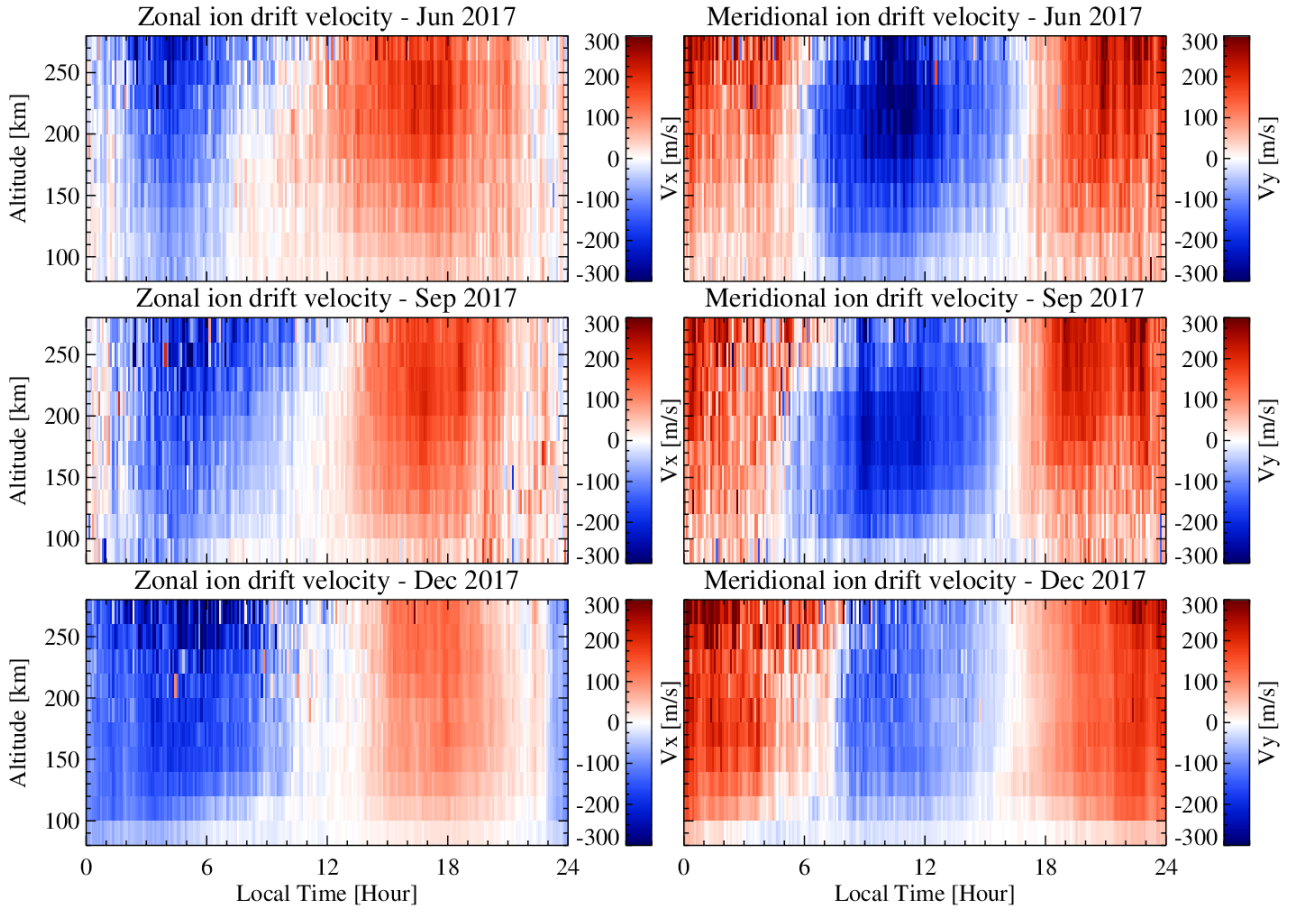

Fig. 10. Diurnal variations of the monthly mean horizontal ion drift velocity in the zonal (left) and meridional (right) direction for Jun (top), September (middle), and December (bottom) in 2017.

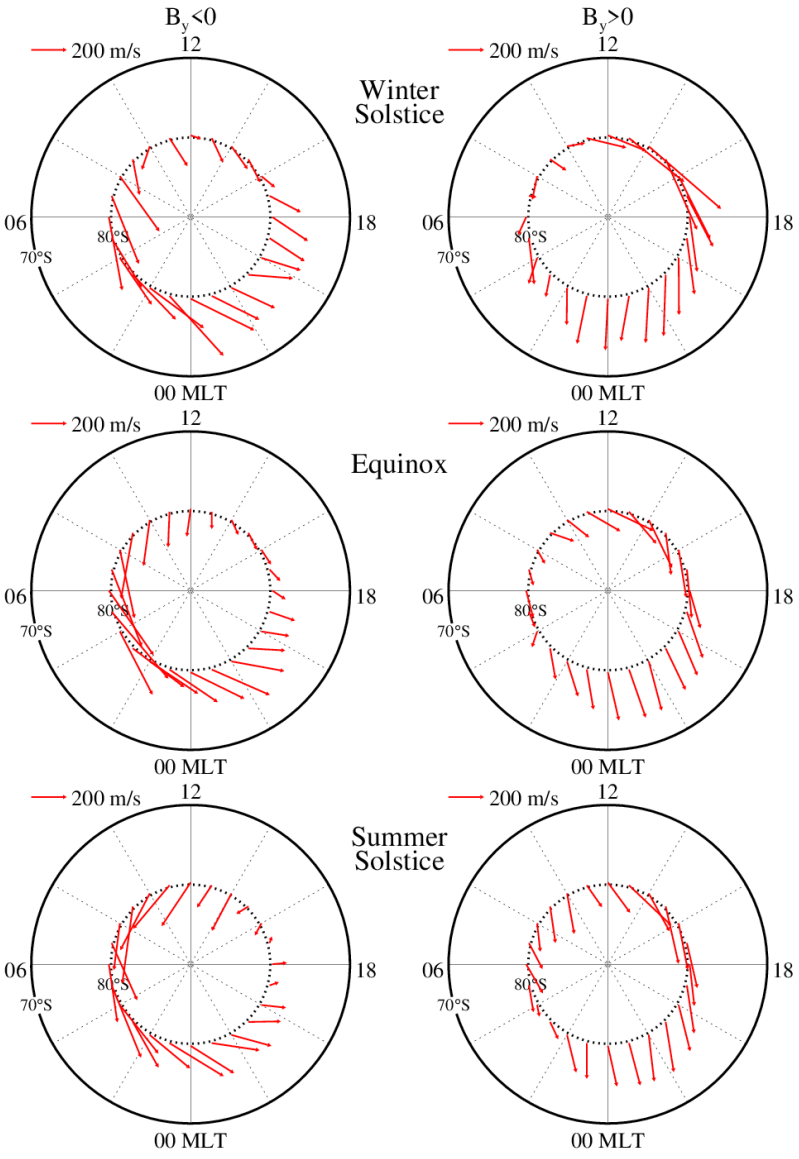

Fig. 11. Hourly mean ion velocity vectors at 250 km altitude from the drift measurements for negative (left) and positive (right) IMF B_y for winter, equinox, and summer in 2017.

the solar wind-magnetosphere-ionosphere interactions. It is well known that the plasma convection affects the neutral atmospheric dynamics through the ion-neutral collision. Since 2014, FPI has been operated at JBS and provides thermospheric neutral wind and temperature measurements. The simultaneous observations of the plasma drift and neutral wind at JBS allow us to make a direct comparison between them. The preliminary result of the comparison is presented in Fig. 12 that shows the monthly mean plasma drift and neutral wind velocities for May, June, July and August in 2017 as depicted in the figure. There exist systematic differences between the ion and neutral motions, which needs to be further studied.

8. CONCLUSIONS

In this paper we introduced the fundamentals of the Dynasonde ionospheric sounding system which was installed at Jang Bogo station in 2015, in comparison with more conventional digisonde system, with some of the results and possible applications for the upper atmospheric research in the southern polar region. The JBS-VIPIR routinely monitors the state of the polar ionosphere over JBS, Antarctica to produce the various ionospheric parameters such as the height profiles of electron density, ion drift, and tilts in the bottomside ionosphere with an unprecedented temporal resolution. Compared to the Arctic region, there

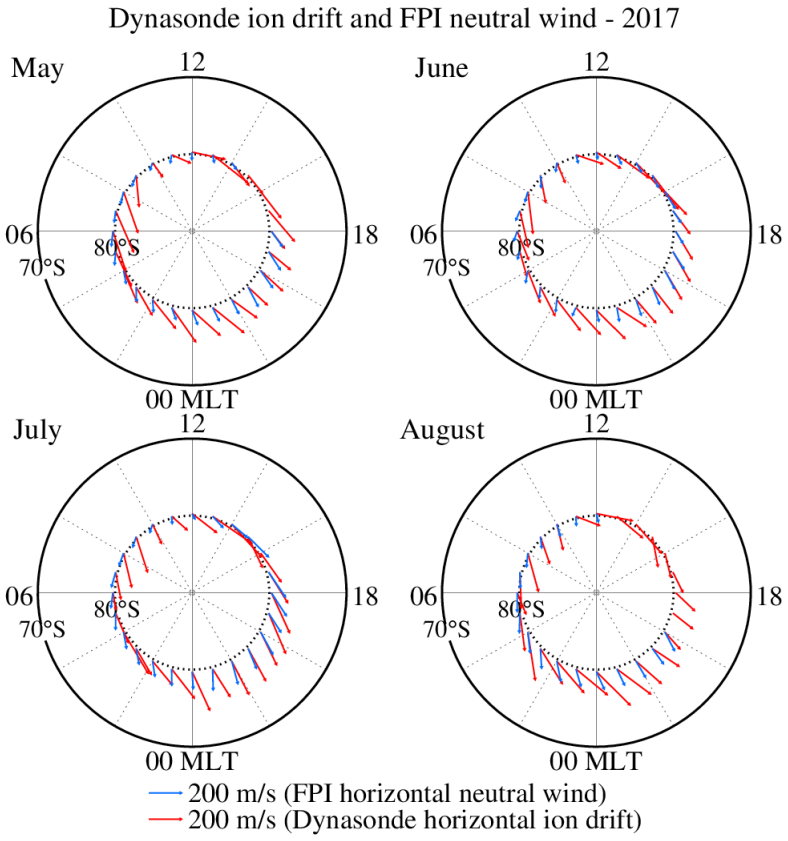

Fig. 12. Comparison between the averaged VIPIR ion drift (red) and the FPI neutral winds (blue) for May, June, July and August in 2017.

are relatively limited observations performed in Antarctica due to the very limited accessibility. Thus the high-resolution ionospheric data from the JBS-VIPIR will provide unique and valuable opportunities for studies on the polar ionosphere in combination with simultaneous observations for the aurora, the neutral atmosphere and the magnetosphere at JBS.

ACKNOWLEDGMENTS

This work was supported by the Grant PE20100 from the Korea Polar Research Institute.

ORCID

Young-Bae Ham https://orcid.org/0000-0002-1714-0638
Geonhwa Jee https://orcid.org/0000-0001-7996-0482
Changsup Lee https://orcid.org/0000-0003-4046-7089
Hyuck-Jin Kwon https://orcid.org/0000-0001-9670-0711
Jeong-Han Kim https://orcid.org/0000-0002-8312-8346
Nikolay Zabotin https://orcid.org/0000-0003-0715-1082
Terence Bullett https://orcid.org/0000-0001-9256-6105

REFERENCES

Australian Government Bureau of Meteorology, Ionosonde antennas (1998) [Internet], viewed 2020 Apr 1, available from: http://www.sws.bom.gov.au/IPSHosted/INAG/web-62/ionoso~1.htm

Bullett TW, Redmon RJ, Transmit antenna for ionospheric sounding applications, Proceedings of the XXIXth URSI General Assembly, Chicago, IL, 7-16 Aug 2008.

Chisham G, Lester M, Milan SE, Freeman MP, Bristow WA, et al., A decade of the super sual auroral radar network (SuperDARN): scientific achievements, new techniques and future directions, Surv. Geophys. 28, 33-109 (2007). https://doi.org/10.1007/s10712-007-9017-8

Heelis RA, The polar ionosphere, Rev. Geophys. 20, 567-576 (1982). https://doi.org/10.1029/RG020i003p00567

Huang X, Reinisch BW, Real-time HF ray tracing through a tilted ionosphere, Radio Sci. 41, RS5S47 (2006). https://doi.

org/10.1029/2005RS003378

Kim JE, Kim JH, Jee G, Lee C, Kwon HJ, et al., Ground-based observations for the upper atmosphere at Jang Bogo Station, Antarctica: preliminary results, Curr. Sci. 115, 1674-1678 (2018). https://doi.org/10.18520/cs/v115/i9/1674-1678

Kwon HJ, Lee C, Jee G, Ham Y, Kim JH, et al., Ground-based observations of the polar region space environment at the Jang Bogo Station, Antarctica, J. Astron. Space Sci. 35, 185-193 (2018). https://doi.org/10.5140/JASS.2018.35.3.185

Lee C, Jee G, Wu Q, Shim JS, Murphy D, et al., Polar thermospheric winds and temperature observed by fabry-perot interferometer at Jang Bogo Station, Antarctica, J. Geophys. Res. Space. 122, 9685-9695 (2017). https://doi.org/10.1002/2017JA024408

Lester M, The super dual auroral radar network (SuperDARN): an overview of its development and science, Adv. Polar Sci. 24, 1-11 (2014). https://doi.org/10.3724/sp.j.1085.2013.00001

Lu G, Richmond AD, Lühr H, Paxton L, High-latitude energy input and its impact on the thermosphere, J. Geophys. Res-Space. 121, 7108-7124 (2016). https://doi.org/10.1002/2015ja022294

Negrea C, Zabotin N, Bullett T, Codrescu M, Fuller-Rowell T, Ionospheric response to tidal waves measured by dynasonde techniques, J. Geophys. Res. Space Phys. 121, 602-611 (2016). https://doi.org/10.1002/2015ja021574

NOAA National Centers for Environmental Information, Dynasonde ionosphere explorer (2016) [Internet], viewed 2020 Apr 1, available from: https://www.ngdc.noaa.gov/stp/iono/Dynasonde/

Reinisch BW, Galkin IA, Global ionospheric radio observatory (GIRO), Earth Planets Space 63, 377-381 (2011). https://doi.org/10.5047/eps.2011.03.001

Rishbeth H, Eyken AP, EISCAT: early history and the first ten years of operation, J. Atmos. Terr. Phy. 55, 525-542 (1993). https://doi.org/10.1016/0021-9169(93)90002-g

Russell CT, The polar cusp. Adv. Space. Res. 25, 1413-1424 (2000). https://doi.org/10.1016/s0273-1177(99)00653-5

Sato K, Tsutsumi M, Sato T, Nakamura T, Saito A, et al., Program of the antarctic syowa MST/IS radar (PANSY), J. Atmos. Sol.-Terr. Phy. 118, 2-15 (2014). https://doi.org/10.1016/j.jastp.2013.08.022

Sedgemore KJF, Wright JW, Williams PJS, Jones GOL, Rietveld MT, Plasma drift estimates from the Dynasonde: comparison with EISCAT measurements, Ann. Geophys. 16, 1138-1143 (1998). https://doi.org/10.1007/s00585-998-1138-y

Sergeev VA, Polar cap and cusp boundaries at day and night, J. Geomag. Geoelectr. 42, 683-695 (1990). https://doi.org/10.5636/jgg.42.683

Sulzer MP, RADAR | Incoherent scatter radar, in Encyclopedia of Atmospheric Sciences, eds. North GR, Pyle J, Zhang F (Academic Press, San Diego, CA, 2015), 422-428.

Tuve MA, Breit G, Note on a radio method of estimating the height of the conducting layer, Terr. Magnet. Atmos. Electr. 30, 15-16 (1925). https://doi.org/10.1029/te030i001p00015

Valentic T, Buonocore J, Cousins M, Heinselman C, Jorgensen J, et al., AMISR the advanced modular incoherent scatter radar, Proceedings of the 2013 IEEE International Symposium on Phased Array Systems and Technology, Waltham, MA, 15-18 Oct 2013.

Wright JW, Pitteway MLV, Real-time data acquisition and interpretation capabilities of the Dynasonde: 1. data acquisition and real-time display, Radio Sci. 14, 815-825 (1979a). https://doi.org/10.1029/rs014i005p00815

Wright JW, Pitteway MLV, Real-time data acquisition and interpretation capabilities of the Dynasonde: 2. determination of magnetoionic mode and echolocation using a small spaced receiving array, Radio Sci. 14, 827-835 (1979b). https://doi.org/10.1029/RS014i005p00827

Wu Q, Jee G, Lee C, Kim JH, Kim YH, et al., First simultaneous multistation observations of the polar cap thermospheric winds, J. Geophys. Res. 122, 907-915 (2017). https://doi.org/10.1002/2016ja023560

Zabotin NA, Wright JW, Zhbankov GA, NeXtYZ: three-dimensional electron density inversion for dynasonde ionograms, Radio Sci. 41, RS6S32 (2006). https://doi.org/10.1029/2005rs003352